**RESEARCH ARTICLE**

# Chitosan-coated sand and its application in a fixed-bed column to remove dyes in simple, binary, and real systems

Alisson Schons Camara [1] · Sabrina Frantz Lütke [1] · Cláudio Pereira Pinheiro [1] · Mery Luiza Garcia Vieira [1] ·
Tito Roberto Sant'Anna Cadaval Jr [1] · Luiz Antonio de Almeida Pinto [1]

## Abstract
Adsorption of tartrazine yellow food dye, in a fixed-bed column, was carried out using a single system, a binary system (in the presence of sunset yellow food dye), and in a real effluent provides from an ice cream industry. Chitosan was used to coat sand particles by the dip-coating technique, and these particles were applied in fixed-bed adsorption. The assays were performed in flow rates of 3 mL min$^{-1}$ and 5 mL min$^{-1}$. The best performance was reached at 3 mL min$^{-1}$. In this flow rate, for single and binary systems, the breakthrough time was 95 min and 65 min, and the maximum capacity of the column was around 595 mg g$^{-1}$ and 497 mg g$^{-1}$, respectively. In the assay conducted with the real effluent, the breakthrough time was 10 min, and the maximum adsorption capacity of the column was reduced to 191 mg g$^{-1}$ for tartrazine dye. The dynamic models of Thomas and Yoon-Nelson were used, and both were suitable to represent the breakthrough curves.

**Keywords** Adsorption · Real effluent · Fixed bed · Chitosan · Food dye · Sand

## Introduction

Industrial processes develop a large amount of products, and in parallel, generating effluents, causing problems to human health and environmental. Between the different contaminants, dyes stand out due to the quantity produced and its recalcitrant characteristics. Many treatments for dye removal from wastewaters are available, such as chemical oxidation, reduction, membrane separation, and photodegradation. However, the majority of these techniques shows problems, such as complex and costly maintenance and operation. Thus, adsorption stands out due to its simplicity and low-cost operation (Yagub et al. 2014; Hassan and Carr 2018; Marques et al. 2018; Alves et al. 2019; Ye et al. 2017, 2019a, b, 2020). Batch adsorption is not ideal for industrial processes, due to the separation problems between adsorbent and adsorbate and by the difficulty to treat large liquids volumes. Thus, fixed bed emerges as an alternative, by its ability to treat large effluent volumes continuously (Gong et al. 2015; Brion-Roby et al. 2018).

Chitosan is a bioproduct that can be obtained from crustacean shells. The primary amines, present in the chitosan structure, can be protonated in acid medium, creating a cationic aspect and conferring high adsorption capacity for the anionic molecules (Auta and Hameed 2014; Gonçalves et al. 2018; Marques Jr. et al. 2018; Farias et al. 2019; Affonso et al. 2020). Anionic dyes have acidic groups, such as, $SO_3H$ and $COOH$, which established bonds between protonated $-NH_3^+$ group of chitosan and acid group of dye. Usually, chitosan presents particulates with very small diameters, causing the bed obstruction. Thus, it is necessary to change the chitosan, and a manner is the production of chitosan beads, which consists of dripping chitosan diluted in an alkaline solution. However, the chitosan beads have a poor mechanical strength and dissolve in acidic medium, so they cannot be used with anionic dyes (Kim et al. 2012). The coating of inert particles with chitosan enables its use in fixed beds and in a wide pH range (Pal et al. 2013; Vieira et al. 2014; Vieira et al. 2019). Sand is a good material to be coated with chitosan due to the abundance of

[1] School of Chemistry and Food, Federal University of Rio Grande–FURG, km 8 Italia Avenue, Rio Grande, RS 96203–900, Brazil

anionic silicate groups, such as $SiO_4^{4-}$, which can interact with the protonated groups of chitosan (Putnis 1995). In this way, sand coated with chitosan can be a great adsorbent for a fixed bed to treat effluents with dyes. The chitosan coating on different materials has been reported by several works as a promising adsorbent, such as bentonite beads coated with chitosan used in the indium ion removal (Calagui et al. 2014); cellulose microfibers coated by chitosan/titanium oxide nanocomposite (Tahseen et al. 2016); glass plate coated by cross-linked chitosan/epichlorohydrine employed for dye removal from wastewater in batch systems (Jawad et al. 2017); bentonite, sand, and kaolinite coated with chitosan employed in copper Cu(II) removal (Futalan et al. 2019); and glass beads, porcelain beads, and polyethylene pellets coated by chitosan used in dyes removal from aqueous solutions in fixed-bed systems (Vieira et al. 2014; Pinheiro et al. 2019).

Commonly, food industries use more than one dye at the same time in their formulation. Consequently, the wastewaters present different dyes, and the development of studies applying matrix effects in the system is important. Thus, the aim of this work was to study the adsorption of tartrazine yellow food dye in a single system, in binary systems (in the presence of sunset yellow food dye), and in a real effluent from an ice cream production industry, using sand coated with chitosan in a fixed-bed column. The effect of flow rate on the breakthrough curves was investigated, and Thomas and Yoon-Nelson models were fitted to the experimental data.

## Material and methods

### Material

Sand (particle size of 1.00 mm, sphericity of 0.75, and density of 2150 kg m$^{-3}$) was purchased in local commerce in the city of Rio Grande, Brazil. Chitosan (molecular weight of $147 \pm 5$ kDa, deacetylation degree of $85 \pm 1\%$, and mean diameter of $72 \pm 3$ μm) was obtained from shrimp wastes (*Penaeus brasiliensis*) according to Weska et al. (2007).

Tartrazine yellow dye ($C_{16}H_9N_4Na_3O_9S_2$, FD&C yellow 5, color index 19,140, molecular weight 534.4 g mol$^{-1}$, λ 425 nm, dye content of 90.0%) and sunset yellow dye ($C_{16}H_{10}N_2Na_2O_7S_2$, FD&C yellow 6, color index 15,985, molecular weight 452.4 g mol$^{-1}$, λ 480 nm, dye content of 90.0%) were supplied by Duas Rodas Ind. (Brazil). Acetic acid ($CH_3COOH$) was purchased from the Qhemis company (Brazil) with a minimum content of 99.7%, and sodium hydroxide (NaOH) was purchased from the Sigma-Aldrich company (Brazil) with a minimum content of 99.0%. The real effluent was obtained from an ice cream local industry in the city of Rio Grande, Brazil, and presented pH of 3.0 and concentration of 89.5 mg L$^{-1}$ of tartrazine dye and of 17.1 mg L$^{-1}$

of sunset dye. The matrix of the effluent was composed of sugars, flavorings, stabilizers, thickeners, and emulsifiers.

### Preparation and characterization of sand coated with chitosan

The sequential steps of cleaning, coating application, and cure were used in the sand coating. Firstly, the cleaning was realized by immersion of 100 g of sand in 100 mL of acetic acid 3% (v/v) at room temperature ($25 \pm 2$ °C) for 6 h. After, the sand was separated from the solution by filtration and dried at temperature of $50 \pm 2$ °C for 24 h. The dip-coating technique was used to coat the sand. In this procedure, 100 g of sand was immersed in 100 mL of chitosan solution (0.5 g of chitosan in 100 mL of acetic acid 3% (v/v), for 12 h at room temperature ($25 \pm 2$ °C). The sand coated was filtered, and the physicochemical cure method was used. In this step, the coated sand was immersed in 1.0% NaOH solution, for 4 h, for chitosan coagulation. Subsequently, it was washed with distilled water until neutral pH; afterward, the sand was dried. Some additional care was taken during the physical curing step (drying). The sand coated with chitosan was dried at 50 °C for 24 h, in trays 30-cm length and 22-cm width. In this way, a large sand surface area coated with chitosan was exposed, contributing to the drying process. To ensure the results, moisture content tests to constant weight were performed, only with sand and with sand coated with chitosan. Thus, it was possible to verify the chitosan mass present (adhered) in each gram of sand. To determine the chitosan mass adhered, the coated sand was weighed after the coating procedure in an analytical balance (Marte, model AY220, Brazil). The coating assays were carried out in three replicates ($n = 3$).

The chitosan mass coated by sand initial mass ($C$) was given by a relation between the coated sand mass, $m_{CS}$ (g), and the sand initial mass, $m_S$ (g), according to Eq. (1). This value was used to assist in determination of the mass of adsorbent contained in the adsorption column:

$$C = \frac{m_{CS} - m_s}{m_s} \tag{1}$$

In addition, the chitosan mass adhered on sand was determined by two more methods: by moisture content test on samples of sand and sand coated with chitosan, according to the methodology described by AOAC (1995), and by determination of chitosan concentration in the coating solution remaining, through methodology adapted from Muzzarelli (1998), according to previous work (Vieira et al. 2014).

The textural characteristics of sand, before and after coating with chitosan, were observed by scanning electron microscopy (MEV) (JEOL, model JSM 6610LV, Japan), and the elemental composition was obtained by dispersive energy spectroscopy (EDS) (JEOL, model JSM–5800, Japan).

## Application of coated sands in fixed-bed adsorption

The coated sand was applied for adsorption in fixed-bed column. For the adsorption experiments, an acrylic column (internal diameter of 3.4 cm and height of 30.0 cm) was used, which was packed with 130 g of coated sand, corresponding to a height of 10 cm, coupled to a peristaltic pump (MasterFlex, model number 07553-75, Canada). Glass beads with an average diameter of 1 mm were used for the base of the column. Before the experiments, it was evaluated the interaction of the support material (sand grains) with the dyes in solution. It was observed that the sand grains did not adsorb the dyes in a quantity able to be detected in the spectroscopy analysis. The experiments were performed in *single* and *binary systems* and, also, using the real effluent from ice cream industry. The single system initial concentration was 90.0 mg L$^{-1}$ of tartrazine yellow dye, and the binary system initial concentrations were 90.0 mg L$^{-1}$ of tartrazine yellow dye and 20.0 mg L$^{-1}$ of sunset yellow dye. The pH value of dye solutions was adjusted at 3.0 with buffer disodium phosphate/citric acid solution. The solutions were pumped upward through the column at flow rates of 3 mL min$^{-1}$ and 5 mL min$^{-1}$. The flow variation was performed to verify if the contact time would generate a relevant change of the bed adsorption capacity, since the higher the flow, the less contact time exists between the dye molecules and the adsorbent biopolymer surface. However, regarding the industrial application, it is interesting to be able to work with the highest possible flow, increasing the treatment capacity in terms of volume, improving operation efficiency. The temperature used for all experiments was 25 °C, since the treatment of effluents is carried out, in general, at room temperature, aiming at cost reduction and operational ease.

At the column top, samples were collected at regular time intervals until the bed exhaustion (outlet concentration equals the inlet concentration). The dye concentration was determined by spectrophotometry (Quimis, model Q108 DRM, Brazil) in the wavelengths of 425 nm and 480 nm for the tartrazine yellow dye and sunset yellow dye, respectively. In the real effluent, the dye concentration measurements were performed using the standard addition method. For this, aliquots of the same volume of the real effluent were added in a volumetric flask. Then, increasing volumes of the standard dye solution at a given concentration were added to reach final dye concentrations ranging from 5 to 25 mg L$^{-1}$. Also, a blank sample was prepared, without the standard dye solution. After preparing the solutions, the spectrometric determination was performed at the referred wavelength, and the standard addition calibration curve was obtained. The tartrazine yellow dye and sunset yellow dye concentrations in the binary system were

calculated by Eqs. (2) and (3), respectively (Gonçalves et al. 2018):

$$C_A = \frac{k_{B2}d_1 - k_{B1}d_2}{k_{A1}k_{B2} - k_{A2}k_{B1}} \tag{2}$$

$$C_B = \frac{k_{A1}d_2 - k_{A2}d_1}{k_{A1}k_{B2} - k_{A2}k_{B1}} \tag{3}$$

where $k_{A1}$, $k_{A2}$, $k_{B1}$ e $k_{B2}$ are the molar absorptivities of tartrazine yellow dye (A) and sunset yellow dye (B) in the wavelengths of 425 nm ($\lambda_1$) and 480 nm ($\lambda_2$), respectively, and $d_1$ e $d_2$ are the absorbance values of tartrazine yellow dye and sunset yellow dye, respectively.

The data were expressed as breakthrough curves ($C_t/C_0$ vs. t). The breakthrough time ($t_b$) and exhaustion time ($t_e$) were determined when the dye concentration ($C_t$) at the column top reached 5% and 95% of the initial dye concentration ($C_0$), respectively (Lemus et al. 2017). The amount of dye adsorbed in the fixed-bed column, $m_{ad}$ (mg), was obtained according to Eq. (4) (Geankoplis 1998; Esfandian et al. 2017; Brion-Roby et al. 2018):

$$m_{ad} = \frac{Q}{1000} \int_{t=0}^{t=total} C_{ad} dt \tag{4}$$

where $t_{total}$ is the total flow time (min), $Q$ is the volumetric flow rate (mL min$^{-1}$), $C_{ad}$ is the adsorbed dye concentration (mg L$^{-1}$), and the integral is the area below the breakthrough curve ($1-C_t/C_0$) vs. t.

The equilibrium dye uptake or maximum capacity of the column, $q_{eq}$ (mg g$^{-1}$), the total amount of dye in the column, $m_{total}$ (g), and the dye removal percentage, $R$ (%), are calculated by Eqs. (5) to (7) (Brion-Roby et al. 2018; Esfandian et al. 2017).

$$q_{eq} = \frac{m_{ad}}{m} \tag{5}$$

$$m_{total} = \frac{C_0 Q T_{total}}{1000} \tag{6}$$

$$R(\%) = \frac{m_{ad}}{m_{total}} 100 \tag{7}$$

where $m$ is the mass of chitosan in the column (g), $C_0$ is the influent concentration (mg L$^{-1}$), and $t_{total}$ is the total flow time (min).

The mass transfer zone (MTZ) is the bed region where the concentration is changing, and thus, the mass transfer is occurring. The mass transfer zone (MTZ) was calculated from Eq. (8), where $h$ is the height of the column (cm):

$$MTZ = h\left(1 - \frac{t_b}{t_e}\right) \tag{8}$$

## Thomas dynamic model

Thomas model predicts the capacity of the adsorbent using important parameters of the process, as with the flow rate, effluent volume, and adsorbent mass. The concept of this model is the Langmuir isotherm and the pseudo-second order kinetic model, without axial dispersion, as represented by Eq. (9):

$$\frac{C_t}{C_0} = \frac{1}{1 + \exp\left(\frac{K_{Th}}{Q}(q_e m - C_0 V_{eff})\right)} \tag{9}$$

where $C_t$ is the effluent concentration (mg L$^{-1}$), $C_0$ is the influent concentration (mg L$^{-1}$), $Q$ is the flow rate (mL min$^{-1}$), $K_{Th}$ is the Thomas kinetic constant (mL mg$^{-1}$ min$^{-1}$), $V_{eff}$ is the effluent volume (mL), $q_e$ is the maximum capacity of the adsorbent (mg g$^{-1}$), and $m$ is the adsorbent mass (g).

## Yoon Nelson dynamic model

Yoon and Nelson correlated the decreasing rate of the adsorption for each molecule of adsorbate with the breakthrough of the adsorbent, showing that this is proportional (Eq. (10)). This model enhances the answers to lower and higher breakthrough curve times determined by Thomas model (Patrick and Cosmas 2016):

$$\frac{C_t}{C_0} = \frac{1}{1 + \exp(K_{YN}(\tau - t))} \tag{10}$$

where $C_t$ is the effluent concentration (mg L$^{-1}$), $C_0$ is the influent concentration (mg L$^{-1}$), $K_{YN}$ is the Yoon-Nelson kinetic constant (min$^{-1}$), and $\tau$ is the time where 50% of the adsorbent was utilized (min).

## Regression analysis

The parameters were estimated by the fit of the models with the experimental data through nonlinear regression using the Quasi-Newton estimation method. Statistica 7.0 software (Statsoft, USA) was used in the calculations. The fit quality was evaluated by the coefficient of determination ($R^2$) (Eq. (11)) and average relative error (ARE) (Eq. (12)) (Myers and Montgomery 2002):

$$R^2 = \left(\frac{\sum_i^n q_{i,\exp} - \overline{q}_{i,\exp^2} - \sum_i^n q_{i,\exp} - q_{i,\text{model}^2}}{\sum_i^n q_{i,\exp} - \overline{q}_{i,\exp^2}}\right) \tag{11}$$

$$ARE = \frac{100}{v}\sum_1^n \left|\frac{q_{i,\text{model}} - q_{i,\exp}}{q_{i,\exp}}\right| \tag{12}$$

where $q_{i,\text{model}}$ is each value of $q$ predicted by the fitted model, $q_{i,\exp}$ is each value of $q$ measured experimentally, $\overline{q}_{i,\exp}$ is the average of $q$ experimentally measured, and $n$ is the number of experimental points.

# Results and discussion

## Characteristics of sand coated with chitosan

Sand was coated with chitosan solution of 0.5% (w/v) through the dip-coating technique, and the cure was realized by physicochemical method. The coating percentage was 24.5 ± 1.2%. Figure 1 shows the SEM images of sand before and after the coating with chitosan. It can be observed that a decrease in the roughness occurred, with the formation of a homogeneous layer of chitosan on sand surface. Figure 2 shows the EDS spectra obtained. Before coating (Fig. 2a), the major elements were O and Si, since sand is formed by units of SiO$_2$. The element Al can be attributed to the presence of Al$_2$O$_3$. After coating (Fig. 2b), the presence of N was verified. These results confirm the presence of chitosan on sand surface, proving the success of the coating procedure.

## Performance of the fixed-bed column

Figures 3, 4, and 5 and Table 1 show the breakthrough curves and the operations characteristics, respectively, for the single system, binary system, and the real effluent, at flow rates of 3 mL min$^{-1}$ and 5 mL min$^{-1}$. For both flow rates, the single system presented a higher amount of dye adsorbed and the maximum capacity of the column. In the binary system, there are two dyes competing for the active sites of chitosan, so they can be occupied by sunset yellow dye instead of tartrazine yellow dye. Since the two azo dyes have very similar chemical characteristics, such as functional groups and molar masses, the interaction between them and the groups of the biopolymer occurs in a similar way, by electrostatic attraction of the protonated amines groups of chitosan and the sulfonic groups of the molecules of both the dyes. In this context, the reduction of the adsorption capacity presented for the tartrazine yellow dye in the experiments in the binary system becomes proportional to the dyes ratio in the aqueous medium. This same competition among dyes was observed by Gonçalves et al. (2018), who carried out adsorption of tartrazine yellow dye and indigotin blue dye in a batch system. The lowest values of the amount dye adsorbed and maximum capacity of the column, for both flow rates studied, occurred for experiments carried out with the real effluent. This was caused by the competitiveness with other compounds present in the matrix of the real effluent. These other compounds can influence the adsorption by occupying or preventing the dye from approaching the active sites.
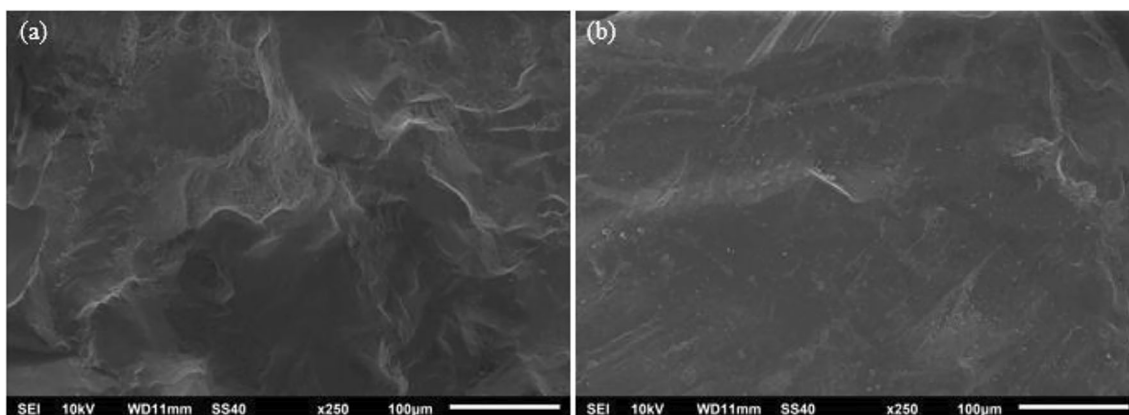
**Fig. 1** SEM images (× 250): (**a**) sand and (**b**) sand coated with chitosan

Regarding the flow rate, the more appropriate results, for experiments realized with the single and binary systems, were obtained for 3 mL min$^{-1}$ (Table 1). This behavior can be attributed to the lower flow rate, which allows a longer time for the dye to interact with the active sites of the chitosan. For the real effluent, contrary behavior was observed. In these systems, there is the presence of another compound, and a lower flow rate can allow a larger quantity of them to occupy or block the active sites, making it difficult to uptake the dye.

The flow rate also affected the breakthrough time. The lower the flow rate, the higher is the breakthrough time (Figs. 3, 4, 5). A greater breakthrough time implies a better adsorption capacity.

In addition, it can be observed in Table 1 that the change of the model system, simple or binary, to the real system leads to a variation in the length of the MTZ. Thus, the length of the column tested was not large enough to have a fully developed profile in the case of the real effluent. This same effect was observed by Sancho et al. (2012), that when studying the

adsorption of emergent compounds in a fixed-bed column, verified that in smaller heights the concentration profile on the bed was not fully developed. At the pH 3 condition, which the experiments were carried out, the biopolymer had its protonated amine groups. In this context and taking into account that the dyes have an anionic character, it is possible to infer that the mechanism of interaction between adsorbent and adsorbate is of the electrostatic type.

## Modeling of breakthrough curves

Table 2 shows the values of Thomas and Yoon-Nelson models' parameters. The coefficient of determination ($R^2$ higher than 0.91) presented similar values for both models. Through the model developed by Thomas, the solute maximum concentration in the adsorbent can be predicted. This information determines whether the column has a good performance; that is, whether the adsorbent has the potential for industrial scale application. When the flow rate was increased (for experiments realized with the single and binary systems), $q_e$ decreases due to the reduction of the contact time between
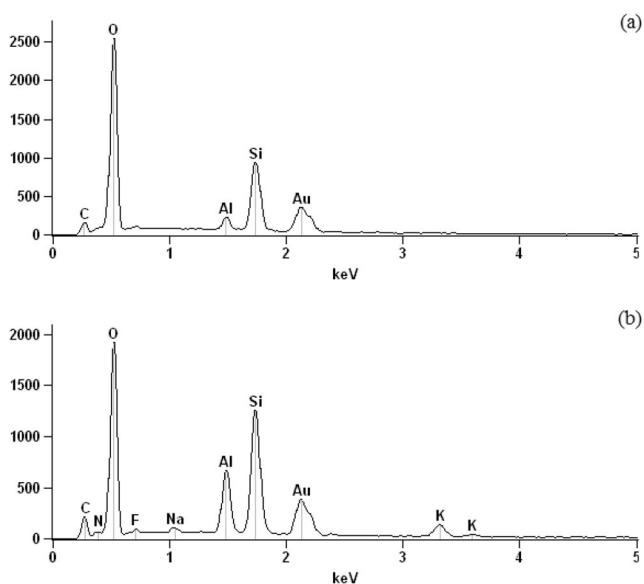


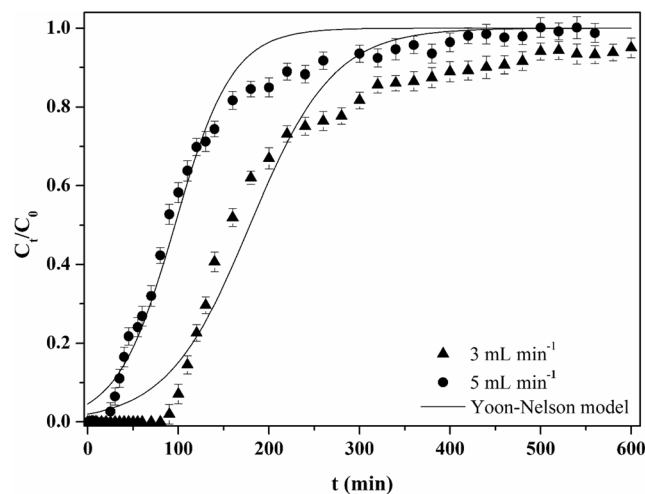**Fig. 2** EDS spectra: (**a**) sand, and (**b**) sand coated with chitosan



**Fig. 3** Breakthrough curves for the adsorption of tartrazine yellow food dye in single system onto sand coated with chitosan
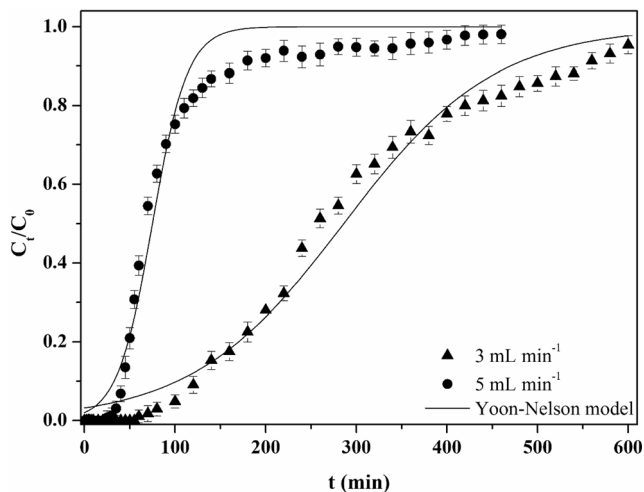
**Fig. 4** Breakthrough curves for the adsorption of tartrazine yellow food dye in binary system onto sand coated with chitosan

the chitosan surface and the dye in solution (Ahmad and Hameed 2010). For the assays realized with the real effluent, this behavior was not observed due to the presence of other compounds. Since the other components present in the matrix too have lower contact time with the adsorbent surface, the active sites are available to the dye adsorption, in a competitive process.

The Yoon-Nelson fit showed that the data for the time where 50% of the adsorption sites are occupied by the adsorbate presented a good correlation between the data predicted and the experimental. The value of the $\tau$ can be related to the adsorption capacity; however, it depends on the system parameters. Higher $\tau$ values could indict higher adsorption capacity. Observing Table 2, this relation occurred, except for the experiments carried out with the single and binary systems at 3 mL min$^{-1}$. For each
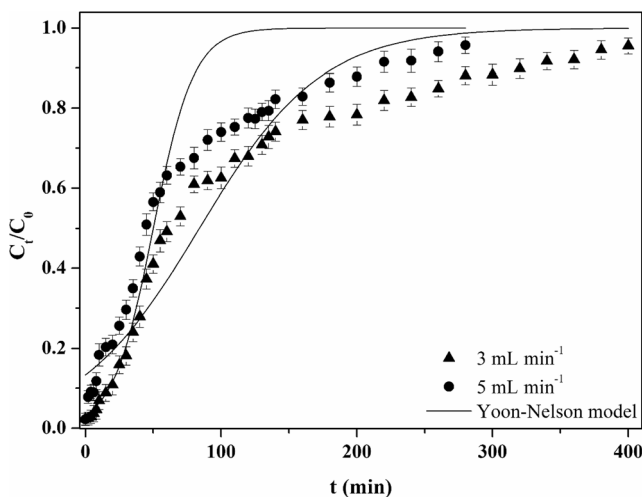


**Fig. 5** Breakthrough curves for the adsorption of tartrazine yellow food dye in real system onto sand coated with chitosan

**Table 1** Operation characteristics for the adsorption of tartrazine yellow food dye in single, binary, and real systems onto sand coated with chitosan

|  | $t_b$ (min) | $t_e$ (min) | MTZ (cm) | $m_{ad}$ (mg)* | $q_{eq}$ (mg g$^{-1}$)* | $R$ (%)* |
|---|---|---|---|---|---|---|
| Flow rate 3 mL min$^{-1}$ | | | | | | |
| Single | 95 | 600 | 8.4 | 94.9 ± 0.8 | 595.3 ± 9.1 | 50.2 ± 2.6 |
| Binary | 65 | 620 | 8.9 | 79.3 ± 0.9 | 497.5 ± 9.8 | 69.9 ± 2.9 |
| Real | 10 | 380 | 9.7 | 30.4 ± 1.2 | 191.2 ± 10.1 | 26.8 ± 3.2 |
| Flow rate 5 mL min$^{-1}$ | | | | | | |
| Single | 30 | 340 | 9.1 | 52.8 ± 0.4 | 334.4 ± 5.5 | 27.9 ± 1.2 |
| Binary | 35 | 340 | 8.9 | 42.9 ± 1.1 | 271.0 ± 6.1 | 22.7 ± 1.3 |
| Real | 2 | 280 | 9.9 | 37.9 ± 1.5 | 237.4 ± 10.8 | 20.0 ± 3.9 |

*mean ± standard deviation ($n = 3$)

condition (single, binary, and real effluent), it can be observed a reduction of the value of the $K_{YN}$, when the flow rate was reduced.

As the Yoon-Nelson model is mathematically analogous to the Thomas model, the coefficients of determination present a similar value for both models. However, its parameters provide differentiated information regarding the adsorption. The values of the $q_e$ parameter estimated by Thomas model for the breakthrough curves were close to the experimental values; thus, the Thomas model can be used to predict some of the experimental data. On the other hand, the time required for 50% adsorption of the Yoon-Nelson model ($\tau$) showed good agreement with the experimental value ($\tau_{exp}$); therefore, this model was adequate to represent the breakthrough curves of this work.

Vieira et al. (2019) studied the application of cyanoguanidine-cross-linked chitosan-coated glass beads in a fixed bed for the FD&C Red 40 dye adsorption. The authors reported that the breakthrough curves with the use of these glass beads coated reached the adsorption capacity values around 80 mg g$^{-1}$. In other work, Vieira et al. (2018) used chitosan with different deacetylation degrees to coat glass beads. The coated beads were applied in fixed bed for tartrazine dye and sunset yellow dye adsorption from aqueous solutions; the authors found that the column maximum adsorption capacities were around 68.7 mg g$^{-1}$ to tartrazine dye adsorption and 75.5 mg g$^{-1}$ to sunset yellow dye. In present work, the maximum capacities of the column for single system and binary system were around 595 mg g$^{-1}$ and 497 mg g$^{-1}$, respectively; for the real effluent, the maximum capacity of the column was 237 mg g$^{-1}$. This decrease in the adsorption capacity can be attributed to the other components presents in the matrix of the effluent such as sugars, flavorings, stabilizers, thickeners, and emulsifiers.

**Table 2** Dynamic parameters for the adsorption of tartrazine yellow food dye in single, binary, and real systems onto sand coated with chitosan

| | Thomas model | | | Yoon-Nelson model | | |
|---|---|---|---|---|---|---|
| | $k_{Th}$ (mL mg$^{-1}$ min$^{-1}$) | $q_e$ (mg g$^{-1}$) | $q_{e\,(exp)}$ (mg g$^{-1}$) | $k_{YN}$ (min$^{-1}$) | $\tau$ (min) | $\tau_{(exp)}$ (min)* |
| Flow rate 3 mL min$^{-1}$ | | | | | | |
| Single | 0.00057664 | 648 | 595 | 0.02179 | 179 | 170 ± 3 |
| Binary | 0.00057934 | 615 | 497 | 0.01195 | 286 | 280 ± 4 |
| Real | 0.00058820 | 266 | 191 | 0.02223 | 84 | 65 ± 5 |
| Flow rate 5 mL min$^{-1}$ | | | | | | |
| Single | 0.00042143 | 378 | 334 | 0.031593 | 96 | 95 ± 2 |
| Binary | 0.00137249 | 298 | 271 | 0.051885 | 75 | 75 ± 4 |
| Real | 0.00070325 | 247 | 237 | 0.067444 | 50 | 48 ± 6 |

*mean ± standard deviation ($n = 3$)

# Conclusion

In this work, sand coated with chitosan was used for adsorption of tartrazine yellow food dye in fixed-bed column, and the matrix effects were elucidated using real effluent. Adsorption assays in a single system, binary system, and real effluent were evaluated at two flow rates. The best results were found at 3 mL min$^{-1}$ for single and binary systems. This behavior can be attributed to the higher residence time of the solution in the column. With regard to the real effluent, contrary behavior was observed since in a lower flow rate, other compounds present in the matrix of the real effluent can easily occupy or blocky the active sites of the chitosan. In the most adequate flow rate, the maximum capacity of the column for single system and binary system was around 595 mg g$^{-1}$ and 497 mg g$^{-1}$, respectively. For the real effluent, in the most adequate flow rate, the maximum capacity of the column reduces to 237 mg g$^{-1}$ due to the competitiveness of other compounds by the active sites of the chitosan. The Thomas and Yoon-Nelson models were suitable to represent the dynamic behavior. Therefore, this work showed that fixed-bed column packed with sand coated with chitosan can be used to remove tartrazine yellow dye from aqueous solutions. Besides that, this work contributes to supply the lack of studies of dye adsorption in binary systems and real effluents using fixed-bed column.

# References

Affonso LN, Marques JL Jr, Lima VVC, Gonçalves JO, Barbosa SC, Primel EG, Burgo TAL, Dotto GL, Pinto LAA, Cadaval TRS Jr (2020) Removal of fluoride from fertilizer industry effluent using carbon nanotubes stabilized in chitosan sponge. J Hazard Mater 388: 122042. https://doi.org/10.1016/j.jhazmat.2020.122042

Ahmad AA, Hameed BH (2010) Fixed-bed adsorption of reactive azo dye onto granular activated carbon prepared from waste. J Hazard Mater 175:298–303. https://doi.org/10.1016/j.jhazmat.2009.10.003

Alves DCS, Gonçalves JO, Coseglio BB, Burgo TAL, Dotto GL, Pinto LAA, Cadaval TRS Jr (2019) Adsorption of phenol onto chitosan hydrogel scaffold modified with carbon nanotubes. J Environ Chem Eng 7:103460. https://doi.org/10.1016/j.jece.2019.103460

AOAC (1995) Official methods of analysis, vol 1, 16th edn. Association of Official Analytical Chemists, Washington, DC

Auta M, Hameed BH (2014) Chitosan-clay composite as highly effective and low-cost adsorbent for batch and fixed-bed adsorption of methylene blue. Chem Eng J 237:352–361. https://doi.org/10.1016/j.cej.2013.09.066

Brion-Roby R, Gagnon J, Deschênes JS, Chabot B (2018) Investigation of fixed bed adsorption column operation parameters using a chitosan material for treatment of arsenate contaminated water. J Environ Chem Eng 6:505–511. https://doi.org/10.1016/j.jece.2017.12.032

Calagui MJC, Senoro DB, Kan CC, Salvacion JWL, Futalan CM, Wan MW (2014) Adsorption of indium(III) ions from aqueous solution using chitosan-coated bentonite beads. J Hazard Mater 277:120–126. https://doi.org/10.1016/j.jhazmat.2014.04.043

Esfandian H, Samadi-Maybodi A, Khoshandam B, Parvini M (2017) Experimental and CFD modeling of diazinon pesticide removal using fixed bed column with cu-modified zeolite nanoparticle. J Taiwan Inst Chem Eng 75:164–173. https://doi.org/10.1016/j.jtice.2017.03.024

Farias BS, Gründmann DDR, Strieder MM, Silveira N Jr, Cadaval TRS Jr, Pinto LAA (2019) Biosorption of glycerol impurities from biodiesel production onto electrospun chitosan-based nanofibers: equilibrium and thermodynamic evaluations. Environ Sci Pollut Res Int 26:28436–28443. https://doi.org/10.1007/s11356-019-04525-3

Futalan CM, Yang JH, Phatai P, Chen IP, Wan MW (2019) Fixed-bed adsorption of copper from aqueous media using chitosan-coated bentonite, chitosan-coated sand, and chitosan-coated kaolinite. Environ Sci Pollut Res. https://doi.org/10.1007/s11356-019-06083-0

Geankoplis CJ (1998) Processos de Transporte y Operaciones Unitarias, 3rd edn. Compañía Editorial Continental

Gonçalves JO, Silva KA, Dotto GL, Pinto LAA (2018) Adsorption kinetics of dyes in single and binary systems using cyanoguanidine-crosslinked chitosan of different deacetylation degrees. J Polym Environ 26:2401–2409. https://doi.org/10.1007/s10924-017-1133-z

Gong JL, Zhang YL, Jiang Y, Zeng GM, Cui ZH, Liu K, Deng CH, Niu QY, Deng JH, Huan SY (2015) Continuous adsorption of Pb (II) and methylene blue by engineered graphite oxide coated sand in fixed-bed column. Appl Surf Sci 330:148–157. https://doi.org/10.1016/j.apsusc.2014.11.068

Hassan MM, Carr CM (2018) A critical review on recent advancements of the removal of reactive dyes from dye house effluent by ion-exchange adsorbents. Chemosp 209:201–219. https://doi.org/10.1016/j.chemosphere.2018.06.043

Jawad AH, Islam MA, Hameed BH (2017) Cross-linked chitosan thin film coated onto glass plate as an effective adsorbent for adsorption of reactive orange 16. Int J Biol Macromol 95:743–749. https://doi.org/10.1016/j.ijbiomac.2016.11.087

Kim T, Park S, Cho S (2012) Adsorption characteristics of reactive black 5 onto chitosan beads cross-linked with epichlorohydrin. J Ind Eng Chem 18:1458–1464. https://doi.org/10.1016/j.jiec.2012.02.006

Lemus J, Moya C, Gilarranz MA, Rodriguez JJ, Palomar J (2017) Fixed-bed adsorption of ionic liquids onto activated carbon from aqueous phase. J Environ Chem Eng 5:5347–5351. https://doi.org/10.1016/j.jece.2017.10.014

Marques JL Jr, Lütke SF, Frantz TS, Espinelli JBS Jr, Carapelli R, Pinto LAA, Cadaval TRS Jr (2018) Removal of Al (III) and Fe (III) from binary system and industrial effluent using chitosan films. Int J Biol Macromol 120:1667–1673. https://doi.org/10.1016/j.ijbiomac.2018.09.13

Marques BS, Frantz TS, Cadaval TRS Jr, Pinto LAA, Dotto GL (2018) Adsorption of a textile dye onto piaçava fibers: kinetic, equilibrium, thermodynamics, and application in simulated effluents. Environ Sci Pollut Res Int:1–9. https://doi.org/10.1007/s11356-018-3587-5

Muzzarelli RAA (1998) Colorimetric determination of chitosan. Anal Biochem 260:255–257. https://doi.org/10.1006/abio.1998.2705

Myers RH, Montgomery DC (2002) Response surface methodology: process and product optimization using designed experiments. Wiley, New York

Pal A, Pan S, Saha S (2013) Synergistically improved adsorption of anionic surfactant and crystal violet on chitosan hydrogel beads. Chem Eng J 217:426–434. https://doi.org/10.1016/j.cej.2012.11.120

Patrick UA, Cosmas U (2016) Studying and modeling dynamic adsorption of lead (II) ion onto fixed bed column of activated carbon of plantain peels and bamboo. Sci J Environ Eng Res. https://doi.org/10.7237/sjeer/115

Pinheiro CP, Mello TG, Vieira MLG, Pinto LAA (2019) Chitosan-coated different particles in spouted bed and their use in dye continuous adsorption system. Environ Sci Pollut Res 26:28510–28523. https://doi.org/10.1007/s11356-019-04905-9

Putnis A (1995) Introduction to mineral sciences. Cambridge University, Cambridge

Sancho JLS, Rodríguez AR, Torrellas SA (2012) Removal of an emerging pharmaceutical compound by adsorption in fixed bed column. Desalin Water Treat 45:305–314. https://doi.org/10.1080/19443994.2012.692062

Tahseen K, Yasir A, Sher BK, Muhammad TSC, Abdullah MA (2016) Dye adsorption and bactericidal properties of TiO₂/chitosan coating layer. Carbohydr Polym 148:153–160. https://doi.org/10.1016/j.carbpol.2016.04.042

Vieira MLG, Esquerdo VM, Nobre LR, Dotto GL, Pinto LAA (2014) Glass beads coated with chitosan for the food azo dyes adsorption in a fixed bed column. J Ind Eng Chem 20:3387–3393. https://doi.org/10.1016/j.jiec.2013.12.024

Vieira MLG, Martinez MS, Santos GB, Dotto GL, Pinto LAA (2018) Azo dyes adsorption in fixed bed column packed with different deacetylation degrees chitosan coated glass beads. J Env Chem Eng 6:3233–3241. https://doi.org/10.1016/j.jece.2018.04.059

Vieira MLG, Pinheiro CP, Silva KA, Lutke SF, Cadaval TRS, Dotto GL, Pinto LAA (2019) Chitosan and cyanoguanidine-crosslinked chitosan coated glass beads and its application in fixed bed adsorption. Chem Eng Commun 206:1474–1486. https://doi.org/10.1080/00986445.2019.1581618

Weska RF, Moura JM, Batista LM, Rizzi J, Pinto LAA (2007) Optimization of deacetylation in the production of chitosan from shrimp wastes: use of response surface methodology. J Food Eng 80:749–753. https://doi.org/10.1016/j.jfoodeng.2006.02.006

Yagub MT, Sen TK, Afroze S, Ang HM (2014) Dye and its removal from aqueous solution by adsorption: a review. Adv Colloid Interf Sci 209:172–118. https://doi.org/10.1016/j.cis.2014.04.002

Ye S, Zeng G, Wu H, Zhang C, Liang J, Dai J, Liu Z, Xiong W, Wan J, Xu P, Cheng M (2017) Co-occurrence and interactions of pollutants, and their impacts on soil remediation - a review. Crit Rev Environ Sci Technol 47:1528–1553

Ye S, Zeng G, Wu H, Liang J, Zhang C, Dai J, Xiong W, Song B, Wu S, Yu J (2019a) The effects of activated biochar addition on remediation efficiency of cocomposting with contaminated wetland soil. Resour Conserv Recycl 140:278–285. https://doi.org/10.1016/j.resconrec.2018.10.004

Ye S, Yan M, Tan X, Liang J, Zeng G, Wu H, Song B, Zhou C, Yang Y, Wang H (2019b) Facile assembled biochar-based nanocomposite with improved graphitization for efficient photocatalytic activity driven by visible light. Appl Catal B 250:78–88. https://doi.org/10.1016/j.apcatb.2019.03.004

Ye S, Zeng G, Tan X, Wu H, Liang J, Song B, Tang N, Zhang P, Yang Y, Chen Q, Li X (2020) Nitrogen-doped biochar fiber with graphitization from Boehmeria nivea for promoted peroxymonosulfate activation and non-radical degradation pathways with enhancing electron transfer. Appl Catal, B 269:118850. https://doi.org/10.1016/j.apcatb.2020.118850